Applications of Second-Harmonic Generation Imaging Microscopy in Ovarian and Breast Cancer

Karissa Tilbury[1] and Paul J. Campagnola[1,2,*]

[1]Department of Biomedical Engineering, [2]Medical Physics Department, University of Wisconsin-Madison, Madison, WI, USA.
*Corresponding author.

ABSTRACT: In this perspective, we discuss how the nonlinear optical technique of second-harmonic generation (SHG) microscopy has been used to greatly enhance our understanding of the tumor microenvironment (TME) of breast and ovarian cancer. Striking changes in collagen architecture are associated with these epithelial cancers, and SHG can image these changes with great sensitivity and specificity with submicrometer resolution. This information has not historically been exploited by pathologists but has the potential to enhance diagnostic and prognostic capabilities. We summarize the utility of image processing tools that analyze fiber morphology in SHG images of breast and ovarian cancer in human tissues and animal models. We also describe methods that exploit the SHG physical underpinnings that are effective in delineating normal and malignant tissues. First we describe the use of polarization-resolved SHG that yields metrics related to macromolecular and supramolecular structures. The coherence and corresponding phase-matching process of SHG results in emission directionality (forward to backward), which is related to sub-resolution fibrillar assembly. These analyses are more general and more broadly applicable than purely morphology-based analyses; however, they are more computationally intensive. Intravital imaging techniques are also emerging that incorporate all of these quantitative analyses. Now, all these techniques can be coupled with rapidly advancing miniaturization of imaging systems to afford their use in clinical situations including enhancing pathology analysis and also in assisting in real-time surgical determination of tumor margins.

KEYWORDS: nonlinear microscopy techniques, second harmonic generation (SHG) imaging microscopy, multiphoton microscopy, breast cancer, ovarian cancer

CITATION: Tilbury and Campagnola. Applications of Second-Harmonic Generation Imaging Microscopy in Ovarian and Breast Cancer. *Perspectives in Medicinal Chemistry* 2015:7 21–32 doi: 10.4137/PMC.S13214.

RECEIVED: January 07, 2015. **RESUBMITTED:** March 01, 2015. **ACCEPTED FOR PUBLICATION:** March 03, 2015.

ACADEMIC EDITOR: Yitzhak Tor, Editor in Chief

TYPE: Perspective

FUNDING: PJC acknowledges support under NSF CBET-1402757 and the National Cancer Institute R01 CA136590-01A1; KT acknowledges support under 5T32CA009206-34. The authors confirm that the funder had no influence over the study design, content of the article, or selection of this journal.

COMPETING INTERESTS: Authors disclose no potential conflicts of interest.

CORRESPONDENCE: pcampagnola@wisc.edu

Introduction

Ovarian and breast cancers account for 31% of all cancer-associated deaths each year despite the respective high 5-year survival rates of 92% and 99% when diagnosed in early stages (Cancer Facts and Figures, 2014). Currently, 61% of breast cancer cases are diagnosed locally, whereas only 15% of ovarian cancers are found before widespread invasion and metastasis. This striking difference is due to the combination of vague, nonspecific symptoms of ovarian cancer and also the lack of effective screening tools (both serum- and imaging-based). To improve the diagnosis and survivorship of both breast and ovarian cancer, we need to better understand the tumor microenvironment (TME), as metastasis can occur while tumors are still small for both cancers. The size scale required to thoroughly probe the TME is dictated by the size of the architecture, which ranges from <100 nm to 1 μm for cellular organelles and 1 μm to tens of micrometers for cells and collagen fibers in the fibrillar extracellular matrix (ECM). Current clinical imaging approaches [ultrasound, computed tomography (CT), positron emission tomography (PET), and magnetic resonance imaging (MRI)] have resolution limits of ~1 mm to several millimeters and are all capable of imaging large tumors but are not sufficient for probing early stage disease and its progression. Historically, cellular-level imaging has been performed in the clinic by pathologists on ex vivo biopsies. This histological analysis remains the "gold standard" and is required for diagnosis, but its accuracy is dependent on the experience and skill of the pathologist. Additionally, histology is limited by the tissue preparation required for light microscopy techniques, in particular requiring optically thin sections (~5–10 μm), making spatial correlations throughout the tissue difficult, potentially resulting in the loss of potentially valuable information regarding the TME.

Fortunately, in the last decade, traditional light microscopy techniques have been combined with nonlinear optical methods, including multiphoton excitation (MPE) and second-harmonic generation (SHG). The methods use visible and near-infrared wavelengths and, as a result, provide the submicrometer resolution necessary to study the architecture of the TME.[1–5] Several studies using combinations of MPE and SHG imaging for ovarian and breast cancer have recently been published and will be highlighted in this perspective. While these tools have not yet been integrated clinically, we will discuss how they have enhanced as our understanding of the respective TMEs in breast and ovarian cancer and how they may eventually be used for this purpose.

Overview of MPE and SHG Microscopy

We will primarily focus on SHG microscopy techniques, as these have high sensitivity and specificity for probing collagen changes in the stroma of both ovarian and breast cancers. However, we will first provide a brief discussion on MPE fluorescence microscopy, specifically two-photon excited fluorescence (TPEF), in probing the TME dynamics. Despite arising from different physics, both techniques provide intrinsic optical sectioning, lack of out-of-plane photobleaching, and deeper depth penetration due to decreased scattering from longer IR excitation wavelengths. The penetration depth of TPEF and SHG in breast and ovarian tissues is primarily limited by scattering in the tissue at the laser wavelength, where this is known as the "primary filter effect". This will be the same for both SHG and TPEF, as the depth will be independent of the excitation mechanism (for two-photon processes). Using ~900-nm excitation, depths of penetration are typically about ~250–300 μm in breast, 100–200 μm in ovarian tissue, and 50–100 μm in cervix. Better penetration will be achieved in less dense organs such as the lung, liver, and kidney. Penetration depth limitations are dominated by the primary filter effect at typical SHG excitation wavelengths. Therefore intravital imaging in breast and ovary requires the use of a surgically implanted imaging window to image the TME. The different physical underpinnings of TPEF and SHG afford simultaneous targeting of cells and collagen within TME.

Multiphoton-excited microscopy. Two-photon excitation (TPE) occurs when an exogenous (ie, organic dye) or endogenous fluorophore [eg, Nicotinamide adenine dinucleotide (NADH) and flavin adenine dinucleotide (FAD)] or expressed fluorescent protein absorbs two photons simultaneously through a virtual state to an excited upper electronic state (S_1 or S_2). The Jablonksi diagram is shown in Figure 1. This process requires high instantaneous power and, as a consequence, absorption is limited to the plane of focus on the microscope, providing intrinsic optical sectioning.[6] Note that this is in marked contrast with confocal microscopy, where a pinhole is required for three-dimensional (3D) imaging, while absorption will occur throughout the specimen. Due to quantum mechanical considerations, the fluorescence emission properties (spectrum and lifetime) are identical in one- and two-photon absorption. While increased tissue penetration is often cited as a primary advantage of using MPE, the method carries other advantages. For example, significantly greater sensitivity is achieved, as the confocal collection geometry is not necessary. This enables imaging of weak absorbing/emitting species such as FAD and NADH for endogenous visualization of cells and also metabolic analysis, as will be shown below.

The experimental setup is typically built around a confocal laser-scanning microscope with some modifications, including the addition of a high-repetition-rate mode-locked laser.[7] This setup also affords the use of fluorescence lifetime microscopy (FLIM).[8] Fluorescence lifetimes are largely independent of the fluorophore concentration and are sensitive to cellular metabolic states, protein–protein interactions, and protein–DNA interactions in the TME.[9,10] FLIM can be exploited for cancer imaging because tumor cells have metabolic profiles different from those of normal epithelial cells and FLIM can be used for their differentiation.[9–12] For example, Williams et al investigated the metabolism through the measurement of the redox ratio of the endogenous fluorophores NAD(P)H and FAD and found that normal tissues had higher aerobic mitochondrial metabolism than diseased tissues.[11,13] Using limited patient samples, women with *BRCA1* and/or *BRCA2* mutations (who are at a 30-fold increased risk of developing ovarian cancer) were found to have the most variable redox rates, suggesting its use as a potential surveillance method to capture the early cellular changes in the TME.[11] Differences in fluorescent lifetimes have also been found in both the MMTV-PyMT breast cancer model and human breast cancer slides, with tumors cells expressing longer lifetimes.[9] In addition to these lifetime measurements, autofluorescence from these endogenous species is often combined with SHG imaging to provide the cellular context in the fibrillar ECM.

Second-harmonic generation. SHG is a coherent process in which two photons are upconverted to exactly twice the frequency (half the wavelength) of the excitation laser. The first biological SHG imaging was reported in 1986 by Freund using rat tail tendon with a resolution of ~50 μm.[14] Much later, Mohler and Campagnola implemented a practical SHG tissue imaging approach with high resolution and rapid data acquisition.[2] These advances have greatly increased the use of SHG as a powerful imaging modality (see Refs [15–17] and references therein). SHG creation is governed by the nonlinear susceptibility tensor χ^2, which requires a noncentrosymmetric assembly of the "harmonophores" and thus has a permanent dipole moment, on the size scale of λ_{SHG}. These constraints limit the utility of SHG to imaging collagen, myosin, and microtubule assemblies.[2] The primary application of SHG in imaging cancer lies in probing the collagen architecture and determining how it is altered from normal tissues. In general, collagen remodeling occurs in all epithelial cancers, where the specific changes in organization are different in different tumors: eg, alterations can occur in the form of collagen content and/or fibrillar morphology. Fibrillar collagen has a hierarchical structure in which individual procollagen molecules are comprised of a ~300-kDa triple helix in which three α-chains are hydrogen-bonded to each other. The procollagen molecules are covalently linked into fibrils with a diameter of ~20–250 nm, which then are covalently linked to form fibers on the order of ~500 nm in diameter. The hierarchical structure of the collagen fiber, the structure observed in the SHG microscope, aligns well with the size scale of λ_{SHG}, allowing both molecular and supramolecular information to be encoded within the SHG signal. The primary component of the ECM is Col I, which is the most abundant protein in the body, but other isoforms (III, V, VI) are part of the normal

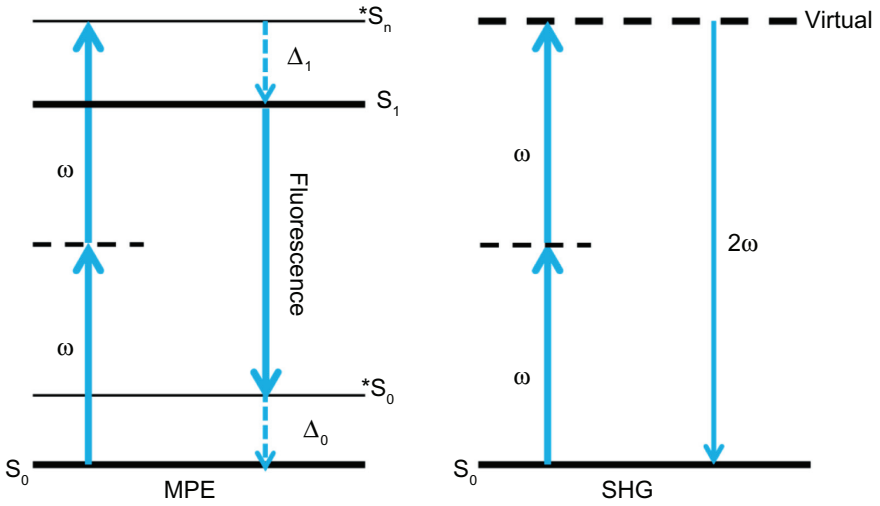

Figure 1. Jablonski energy diagram for MPE and SHG. Energy lost in MPE is signified by Δ_1 and Δ_0. S_0 is the ground state; $*S_0$ is the vibrationally excited state S_0 state; S_1 is the lowest singlet excited state; $*S_n$ ($n \geq 1$) is a vibrationally excited lowest or higher singlet excited state. The excited level in SHG is virtual and in general does not correspond to a real state. Thick arrows represent excitation wavelength, and thinner arrow labeled 2ω is the harmonic response. Dashed lines represent virtual electronic states.

ECM architecture and their relative abundance can change in breast[18] and ovarian cancers.[19]

Morphological Assessment of the Tumor Microenvironment

In pathology, slides are routinely stained with hematoxylin and eosin (H&E), which label nuclei and protein content, respectively, for ready detection of alterations present primarily in cancer cells, such as loss of monolayer cellular organization, change in cell shape, change in nucleus to cytoplasmic ratio, presence of nucleoli, and chromatin condensation. Historically, pathologists have focused primarily on these aspects of cell morphology, and have not typically examined the ECM composition and structure in detail. This is a lost opportunity, as significant remodeling occurs in almost all epithelial cancers. Recently, several research groups have investigated the potential of SHG microscopy using histology slides or intact tissues from human patients and have shown the ability to discern normal from diseased tissue using both cellular and collagen features of the TME.[9,11,12,20–31] Here, we highlight some recent studies using SHG microscopy of breast and ovarian cancer tissues that have focused specifically on either the collagen morphology or this morphology in relationship to the cellular organization. Table 1 provides a summary of the applicability, strengths, and weaknesses of several techniques.

Fourier transforms. Fiber alignment on a global scale or whole field of view without boundaries is routinely performed using the two-dimensional (2D) fast Fourier transform (FFT). This transform determines the spatial frequency components in the image and maps the probability of their occurrence. For example, the 1D FFT of identical fibers would have a single-valued FFT. In addition to the distribution of frequencies, the 2D FFT can also provide alignment assessment. For example, the FFT of randomly orientated fibers has a circular response, whereas aligned fibers have an elliptical FFT. Several research groups have used 2D FFTs either as the sole output in their analysis or as a component to be used in a support vector machine (SVM) learning classification of breast and ovarian tissues.[11,13,28,30,32] Falzon et al presented a unique multistep FFT approach to SHG images of breast cancer. First, collagen fibers within the regions of interest (ROIs) were identified by segmentation.[25] Then, principal component analysis (PCA) of the 2D FFT coefficients was used to quantitatively describe the collagen fiber shape within normal, benign, and malignant breast cancer tissues. This approach was able to classify normal stroma from hyperplasia, dysplasia, and malignant breast cancer, where the last had the most ordered collagen fiber orientation.[25] Similarly, in ovarian cancer tissues, 2D FFT analysis was able to differentiate normal stroma from cancer but was unable to differentiate the type of ovarian cancer, ie, serous, mucinous, endometrioid, and mixed adenocarcinomas.[28,31,32] Two-dimensional FFT analysis of SHG images of both breast and ovarian cancers provide the ability to discern a more organized fibrillar collagen structure in cancerous tissue. However, as a stand-alone method, the technique is unable to detect the slight differences that are often present in the different types of cancers.

Texture analyses. The use of texture analyses has also been investigated in the analysis of SHG images of breast and ovarian cancer. In general, texture considers how the morphology in one part of an image relates to that of its neighbors. The simplest form of texture analysis is the gray-level co-occurrence matrix (GLCM), first developed by Haralick.[33] This approach determines the texture via measuring

Table 1. Comparison of morphological collagen image analysis tools.

ANALYSIS TOOL	PROS	CONS
2D FFT	• No boundaries required; • Widely available in image analysis packages (ie, FIJI, Matlab)	• Not sensitive in detection of small alterations in tissues without a prominent fiber alignment; • Global analysis
Curvelets	• Extraction of individual collagen fibers relative to cellular boundary; very powerful in studying breast cancer progression	• Requires tumor/cell boundary; may not be applicable to other cancer types
GLCM	• Simple geometric relationships based on intensity; • Plug-in available in FIJI	• Highly dependent on fiber orientation; • Low sensitivity and specificity in applications to date
Textons	• Customizable filters, independent of fiber size and intensity	• Large image sets required; • Filters are abstract; • Difficulty in implementation

the gray level of pixels oriented 0°, 45°, 90°, and 135° from an individual pixel or group of pixels. The gray levels of these neighbors are recorded in a matrix, in which mathematical relationships such as the correlation function, entropy, homogeneity, and energy can be used to describe the texture of the image. For example, correlation is useful in detecting the regularity of a particular structure, homogeneity is the weighted sum of the pixel values and provides a metric of similarity of the pixel with its neighbors, and entropy describes the randomness of regions relative to their neighbors. In terms of SHG image analysis in cancer, several studies have used GLCM correlation function analysis and found that normal tissues had a different correlation than abnormal tissues, which corresponded to distinct fibers and less fibrillar structure in normal and abnormal tissues, respectively.[11,28,31,32] In a more detailed analysis, Watson et al successfully combined the GLCM and 2D FFT into an SVM to describe the tissue remodeling of a mouse model of ovarian cancer with ~80% sensitivity and specificity.[30,34]

Recently, textons, a common computer vision application, has been added to the list of morphology-based image analysis tools.[35] Textons are defined as repetitive patterns with slowly varying local statistical properties that are found within an image and are determined by convolving a group of pixels with a filter set of various shapes and sizes to identify repeating features.[36] Wen et al employed a machine learning algorithm including textons and *k*-means clustering to classify human high-grade, serous ovarian carcinoma from normal stroma with 97% accuracy.[35] Note that this approach does not identify discrete features such as an individual fiber sizes or alignment. However, textons are more versatile than other image transforms (ie, 2D FFT, curvelets, and wavelets) as customizable, intensity-independent filters and may be specifically designed for a unique application.

Curvelet transforms to identify tumor boundaries. Collagen fiber characterization and alignment in relation to the cells was robustly described first by Keely and colleagues.[37] While studying the MMTV-PyMT mouse breast model, Provenzano et al coined the descriptor "tumor-associated collagen signatures" (TACS) to describe characteristic forms of collagen alignment changes. The concept has since been extended to characterize and stage human breast and ovarian samples.[22,24,28] The three forms of TACS are characterized by 1) the presence of dense collagen localized around small tumors during early disease and is characteristic of desmoplasia; 2) collagen fibers that are parallel to the tumor boundary for in situ breast carcinoma; and 3) collagen fibers that are normal to the tumor boundary for invasive disease. Representative images of TACs along with the histograms of the distribution of angles for the latter two cases (courtesy of Keely) are demonstrated in Figure 2.[37] The alignment of the fibers relative to the tumor boundary was automatically determined through the curvelet transform. Unlike FFT, which is a global approach, the curvelet transform analyzes frequency components within an image by local correlation with a predefined filter.[38] The curvelet transform is similar to the more common wavelet transform but intrinsically contains orientation information, which is lost in the latter. More recently, Conklin et al showed that aligned collagen or TACS 3 has prognostic value in human breast cancer patients using a three-person-panel time-intensive manual approach.[24] This has now been automated using a combination of existing fiber identifying algorithms (FIRE)[39] and curvelets in CT-FIRE to provide a more rapid image analysis that is more suitable for the clinical environment.[40] For example, fairly simple slide-based MPE and SHG imaging systems are being developed that rapidly image standard histologically prepared H&E slides, allowing overlapping of classical bright-field and MPE/SHG microscopy images.[22,24,40] This overlap can identify the cellular boundary required for TACS analysis, which is invisible by SHG. The tumor–stromal boundary is readily detectable in breast cancer, making TACS a straightforward and powerful assessment; however, in ovarian cancer this boundary is often not easily identified. Despite this difficulty, Adur et al, with the guidance of an expert pathologist, identified TACS signatures in normal and cancerous human ovarian tissues.[28] Normal ovarian tissues demonstrated a TACS-2 cellular–stromal interface with long, straight, and parallel fibers, whereas malignant tissues primarily had TACS-3 fiber alignment.[28]

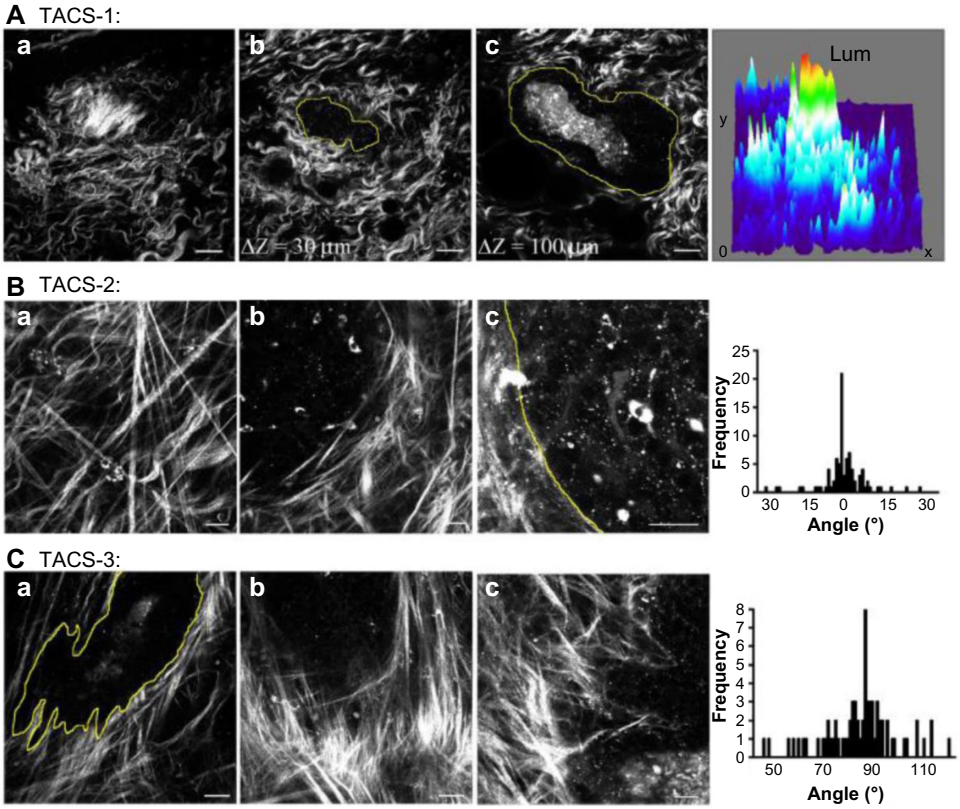

Figure 2. TACS collagen fiber alignment characterization of the MMTV-PyMT breast cancer model accurately characterizes disease progression using SHG microscopy. Adapted from Ref. 37 (courtesy of Patricia Keely).

Morphology-Independent Approaches

The image analysis approaches summarized in Table 1 all rely on the changes in collagen morphology that can be visualized by SHG. While these approaches have been very successful in particular cases, it is also advantageous to have more general approaches in characterizing tissues that do not have regular collagen features that are amenable to these tools. Here we will describe general approaches that exploit the physical underpinnings of SHG contrast to delineate normal and diseased tissues. These are based on the SHG polarization response and SHG emission directionality of different tissues, where both arise from the sub-resolution macromolecular and supramolecular collagen assembly.

Polarization-resolved SHG microscopy. SHG is a second-order process governed by the nonlinear susceptibility tensor χ^2, which is the bulk quantity visualized in the SHG microscope. This arises from coherent summation of the nonlinear response of the collagen molecules, defined by the first hyperpolarizability β, over the size scale of λ_{SHG}. Schanne-Kleinn used hyper-Raleigh scattering measurements to show that the molecular origins of β are due to the coherent amplification of peptide bonds along the length of the collagen molecule.[41] This suggests that the chirality of the collagen triple helix underlies the nonlinear optical response,[42] which is in agreement with our previous interpretation of the SHG polarization dependence arising from the peptide pitch angle of the individual α-helixes in the collagen triple helix.[41,43,44] The ability to probe the structure of the α-helixes within collagen has great potential in probing the TME, as this could serve as another label-free biomarker. This is because different fibrillar collagen isoforms, specifically types I, III, V, and VI, are believed to be upregulated or have higher turnover in breast and ovarian cancers[18,45–48] and, further, have different α-chain incorporations and different net pitch angles. For example, collagen I is a hetererotrimer comprised two $\alpha_1\alpha_2$ chains, whereas collagen III is a homotrimer with three α_1 chains. These are different gene products, and the slight change in the α-helixes (1–2°) can be probed using polarization-resolved SHG microscopy.[44] This is important, as molecular approaches using antibodies often lack specificity between isoforms and, further, can only be used on thin, fixed slides.[45]

Here we provide a description of the SHG polarization response utilized to extract the net pitch angle. The χ^2 tensor has 27 matrix elements. However, using several reasonable approximations, these can be reduced to four nonvanishing elements, where two are degenerate.[49,50] These assumptions include 1) a single axis of hyperpolarizability, ie, β_{zzz} is the only nonvanishing component; 2) well-aligned harmonophores within the focal volume; and 3) Kleinman symmetry, ie, the excitation wavelength is far from resonance (one- or two-photon). Then, the triple-helical collagen molecule is modeled as a cylindrical array of polypeptide coils, where each

α-helix has a peptide pitch angle that can be described as the ratio of tensor elements within χ^2, given by

$$\theta_p = \tan^{-1}\sqrt{\frac{2}{\left(\chi^2_{ZZZ} - \chi^2_{ZZZ}\right)}} \quad (1)$$

This is referred to as the "single-axis molecular model".[43] The first examples using this analysis were limited to well-aligned tissues such as tendon and muscle.[43] However, this treatment is not amenable to the complex morphologies found in the breast and ovarian stroma. Recently, Brasselet and coworkers developed a pixel-based generic model to determine the second-order response of any tissue by analyzing the distribution of dipole moments within the focal volume, where a priori alignment is not required.[51] We integrated this approach into the single-axis molecular model and applied it to a series of mixed Col I/Col III gels as stromal models of ovarian cancer.[44] As shown in Figure 3B, this approach successfully permitted differentiation of these gels, where, for the limiting case of 0% and 40% Col III, we extracted a difference of 0.95°. This small but measurable difference is in agreement with the absolute angle differences of collagen I and III in the Protein Data Bank.[52]

In addition to the peptide pitch angle, this pixel-based approach can determine the alignment of collagen molecules within fibers within the focal volume through measurement of the SHG polarization anisotropy. The SHG anisotropy is defined by the parallel and perpendicular SHG intensity with respect to the laser polarization, as described by

$$\beta = \frac{I_{par} - I_{perp}}{I_{par} + 2I_{perp}} \quad (2)$$

in which β ranges from 0 to 1, and 0 represents completely random organization and 1 represents completely ordered dipole moments. We previously used this for the analysis of entire optical sections or manually on a fiber-by-fiber basis where this resulted in β values of 0.88 and 0.76 for malignant and normal ovarian tissues, respectively.[29] We adapted the pixel-based generic model to determine the SHG anisotropy within fibrils in mixed collagen I/III self-assembled gels. As shown in Figure 3C, we found that the anisotropy values of 100% collagen I was highest at 0° and lowest at 90° relative to the laser polarization, with a reverse trend for 40% collagen III. This result indicates that the dipoles become less aligned within collagen fibrils with increased incorporation of collagen III. The decrease in anisotropy at higher Col III incorporation supports previous structural biology analysis, which showed that collagen I and III molecules co-mingle within single collagen fibrils.[44] While these analyses were performed in fibrillar models, combining the polarization-resolved SHG analysis with the pixel-based anisotropy response has great potential for quantitatively assessing the collagen composition of the breast and ovarian TME.

Two independent research groups have applied polarization-resolved SHG techniques to breast cancer with mixed results. The first such report by Han et al found that the fiber angle relative to the laser polarization in a mouse model of breast cancer was not different in normal versus malignant stroma.[53] A contradictory finding in human breast cancer was reported by Ambekar et al, in which they investigated the $\frac{d_{22}}{d_{31}}, \frac{d_{15}}{d_{31}}$, and $\frac{d_{33}}{d_{31}}$ tensor components. In this study, abnormal fibers were defined as having $\frac{d_{15}}{d_{31}}$ values outside the range of normal fibers. They found the percentage of abnormal fibers to be 10.4%, 19.1%, and 48.8% in hyperplastic, dysplastic, and malignant tissues, respectively.[21] It is notable that, even within the malignant breast tissues, 52.2% of the fibers were considered "normal". Therefore, it is important to have a robust localized method to precisely detect these changes, and we suggest that polarization analysis using the generic model could possibly resolve these differences. Still, despite these conflicting reports and experimental complexity, it is anticipated that polarization-resolved methods will gain increased interest in SHG imaging of cancers.

Phase-matching considerations and SHG directionality. Because SHG is a coherent process, phase-matching conditions between the excitation laser and SHG emission must be satisfied, and this can be exploited for structural analysis. The conditions specific to SHG creation in biological tissues are different from those of the more familiar uniaxial doubling crystals in which the SHG is perfectly phase-matched, where ideal phase-matching (eg, type I) can be observed, with $\Delta k = k_{2\omega} - 2k_{2\omega} = 0$, where $k_{2\omega}$ and k_{ω} are the wave vectors for the SHG and incident photon, respectively. As the coherence length is $2\pi/\Delta k$, all the SHG propagates in the forward direction in this scenario. However, this ideal phase matching is found only in a few uniaxial, birefringent crystals [eg, potassium dihydrogen phosphate (KDP) and beta barium borate (BBO)]. While collagen has been described as a nematic liquid crystal,[54] it does not have type I phase-matching conditions. Although it is not necessary to have $\Delta k = 0$ for SHG creation, the momentum between the excitation and SHG waves must be conserved, and for $\Delta k \neq 0$ this results in a distribution of forward and backward emitted components, which we have defined as F_{SHG}/B_{SHG}.[55] We previously developed a model describing how more random structures relative to the size scale of λ_{SHG} result in lower F_{SHG}/B_{SHG} values than aligned fibrillar assemblies.[56] In addition to this emission directionality, the phase mismatch also has implications on the observed SHG intensity. The relative SHG intensity scales as $\sin(m\Delta kL/2)$ (where m is an integer) and thus becomes less efficient for larger phase mismatch, ie, larger Δk values, which correspond to more random structures compared to the length scale of λ_{SHG}.

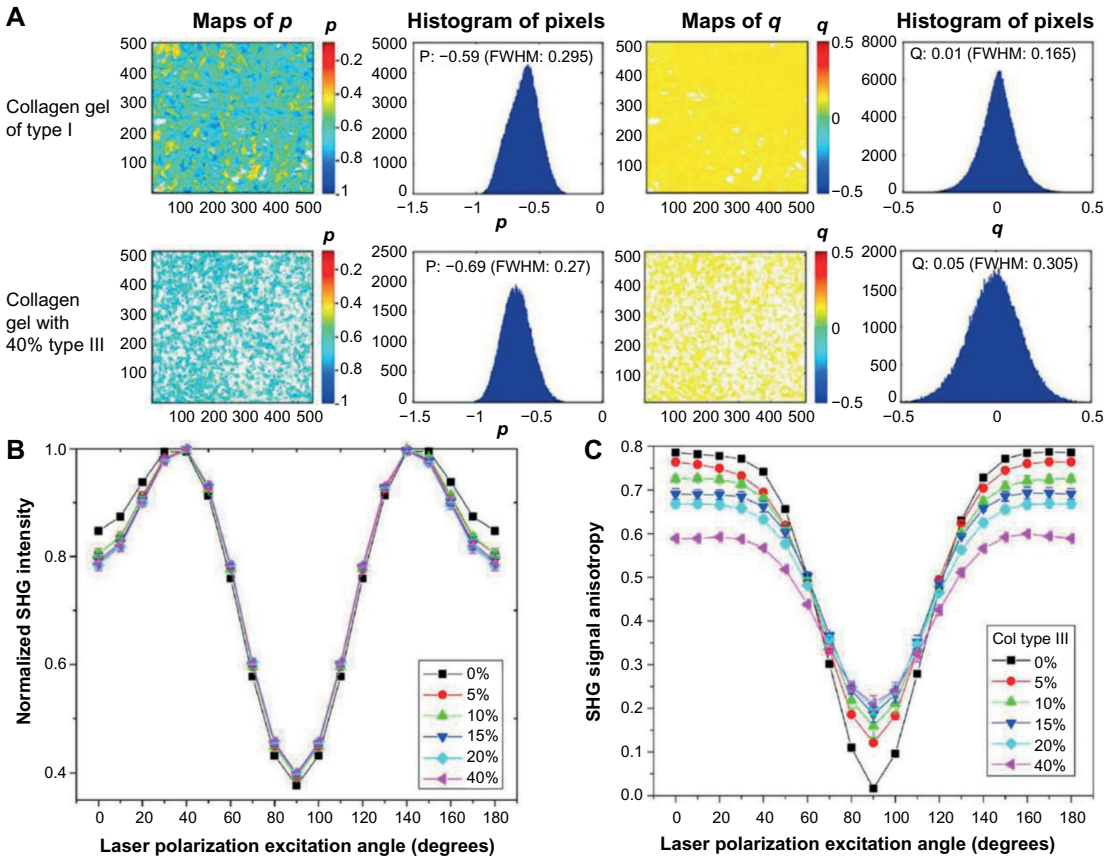

Figure 3. Polarization-resolved microscopy of collagen types I and III. (**A**) Pixel maps of the *p* and *q* values used to minimize the error of dipoles not well aligned within the PSF. (**B**) Simulated SHG intensity response relative to angle is similar to SHG intensity response for the single-molecule model, which when fitted provides the α-helical pitch angle. (**C**) Pixel-based anisotropy response of mixed Col I/III collagen gels using fiber orientation based on *p* and *q* found in panel (**A**). Figure adapted from Ref.[45]

Unlike the previously described morphology-based image processing methods, analysis of collagen organization based on the phase-matching properties (and the corresponding emission directionality) does not rely on the collagen fiber organization, as the SHG creation arises from sub-resolution fibril assembly. Thus, this approach is generalizable and has great potential for clinical applications. As proof of principle, SHG directionality has been studied in self-assembled collagen fibrillar gels with physiologically relevant percentages of collagen III and V to model the upregulation of these collagen types in ovarian and breast cancer, respectively.[44,57] It is believed that, in both cases, collagen III and V co-mingle with collagen I molecules and modulate the fibril size.[45,58] Therefore, these changes in collagen isoform distribution should manifest in altered F_{SHG}/B_{SHG}, and this was indeed observed.[44,57] Specifically, increased fractions of Col III and V resulted in smaller F_{SHG}/B_{SHG} and concurrent lower SHG intensities, both indicative of less efficient phase-matching, ie, greater Δk values, which are reflective of the more random sub-resolution structure.

The fibrillar gels used in the previous studies are essentially nonscattering, and F_{SHG}/B_{SHG} can be determined directly. However, this is not possible in real tissues. In tissue imaging, the measured SHG signal is a convolution of the initially emitted directionality (F_{SHG}/B_{SHG}) and the subsequent scattering of these photons at λ_{SHG}. Scattering in tissues is described by the scattering coefficient μ_s and scattering anisotropy *g*. The former is the inverse of the distance a photon will propagate before undergoing a collision and changing direction, and therefore is a measure of density. The scattering anisotropy *g* (unrelated to the SHG anisotropy β) describes the directionality of the scattering and varies from 0 to 1, with higher values corresponding to greater organization. Differentiation of the coherent SHG directionality F_{SHG}/B_{SHG} and the incoherent components (scattering) is an important consideration for clinical applications because both may be used to differentiate normal from malignant tissues that have changes in fibril size and/or organization.[59] Campagnola and colleagues have developed a technique to extract F_{SHG}/B_{SHG} through a combination of 3D SHG imaging of measured forward to backward ratio (*F*/*B*) as a function of depth into the tissue, independent measurement of μ_s and *g*, and Monte Carlo simulations based on these parameters to model the propagation of the SHG photons. This combined approach affords decoupling of the SHG creation from scattering.[29,59–61] As shown in Figure 4, the optimal Monte Carlo

simulations revealed F_{SHG} best fit values of 93% and 77% for the normal and high-grade ovarian cancer, respectively.[29] We stress that this quantity arises from the sub-resolution fibril structure, and the best fit values are consistent with predictions based on our phase-matching model in conjunction with the corresponding transmission electron microscopy (TEM) images.[29,55] Both normal and malignant ovarian stroma have fibrils that are much smaller in diameter (~60 nm) than λ_{SHG}. However, the malignant stroma has more regularly packed fibrils where this condition is analogous to quasi-phase-matching, resulting in more efficient backward SHG.[62] In sum, this analysis cannot resolve the small fibrils, but the coherence of the SHG permits inferences of organization on this sub-resolution size scale. SHG directionality measurements have also been extended to breast cancer, but the analyses have been inconclusive.[63] This may be because the measurements were taken on thin histological slides and are susceptible to reflections and are also highly sensitive to any slight changes in thickness. In contrast, our combined imaging and simulation method requires tissues of 50–100 µm in thickness to properly account for scattering and are less sensitive to experimental artifacts. In addition, breast tissues are more heterogeneous than the ovarian stroma, which is comprised predominantly of dense collagen. Therefore, additional studies are required to obtain robust knowledge of the SHG directionality alterations associated with normal and malignant breast stroma.

The combined imaging/optical scattering/simulation approach requires several measurements and is computationally intensive; but it is highly general and may be effective in complex fibrillar organization when simpler morphology-based analyses (eg, transforms described earlier) are not applicable. To date, we have found collagen-based tissues have negligible absorption (secondary filter), but we anticipate blood-rich organs will have significant absorption due to the overlap of SHG photons and the absorption spectrum of blood. In performing the SHG emission directionality studies of blood-rich organs, we would account for the increased absorption (measured by integrating spheres) in our Monte Carlo simulations to accurately model the response. An analogous response has long been done in diffuse optical tomography in reconstructing the image.[64] For example, we have used this approach for the analysis of the connective tissue disorder osteogenesis imperfecta[60] and also in the analysis of optical clearing.[61]

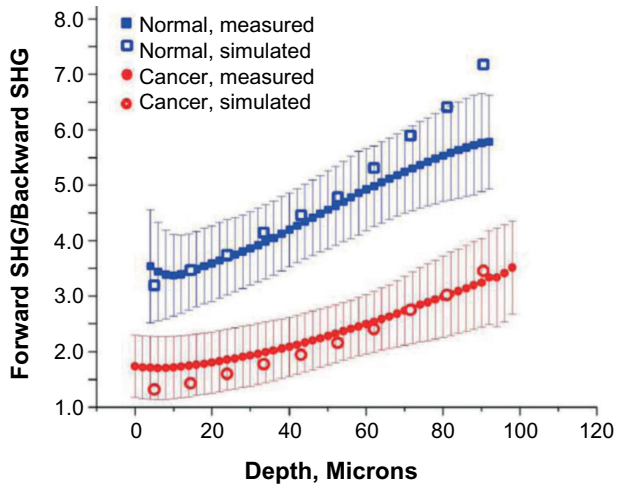

Figure 4. Depth-dependent SHG *F/B* measurements of normal and high-grade serous ovarian cancer. Best fits using Monte Carlo simulations and independently measured μ_s and *g* resulted in 93% and 77% forward-directed SHG in normal and cancer respectively. Adapted from Ref.[30]

To date, TPEF and SHG imaging studies have provided a wealth of information concerning the early ECM alterations associated with breast and ovarian cancers. Tables 2 and 3 summarize the results and conclusions of several papers. Overall, these studies indicate that TPEF and SHG imaging has the sensitivity and specificity to detect early cancerous lesions for both cancers.

Intravital Imaging of Breast and Ovarian Cancer

While analysis of ex vivo tissues can provide great insight (as shown throughout this Perspective), intravital studies in animal models have the potential to yield even greater knowledge, as they permit dynamic imaging of tumor dynamics. Additionally, intravital imaging eliminates tissue preparation steps that may alter the tissue structure. For example, fixing protocols involve tissue dehydration, and the fixative agent adds crosslinks; both may alter the intensity of SHG signal. However, we stress that fixatives do not alter the fibrillar structure. The earliest intravital imaging was demonstrated in 1992 using the dorsal flap method, but it was limited in its ability to mimic human breast cancer, as the mammary environment is not present in the dorsal skin, making study of invasion impossible.[65,66] Furthermore, the xenograft tumors were also limited in their ability to mimic the progression of human disease. However, the combined advent of mammary windows and the MMTV-PyMT mouse model has now permitted progression of the tumor development to be imaged up to 21 days within the same animal.[67] Condeelis found that these windows did not alter the rate of growth in the microenvironment for at least 9 days. Moreover, using stereotactic control with the photoswitchable fluorescent protein Dendra2, the same field of view within the animal was tracked over a period of days.[66,68] Using this approach, they observed amoeboid-like migration of highly invasive breast carcinoma along long ECM fibers (like TACS-3), which were imaged by SHG. By contrast, less invasive cells did not display such directed migration.[66] Additional intravital imaging studies involving xenografts of highly invasive and metastatic human tumor cells demonstrated that stromal cells and cancer cells co-migrate in a single line without cohesive cell junctions but only do so in the presence of tumor-associated fibroblasts.[69] Recent intravital imaging studies have greatly enhanced our understanding of breast cancer and the importance

Table 2. Summary of TPEF and SHG imaging studies and techniques to probe collagen remodeling of the ECM in ovarian cancer.

TECHNIQUE	RESULTS	CONCLUSIONS	AUTHORS
GLCM on SHG images, spatial frequencies + TPEF redox ratios	GLCM $Corr_{50}$ Normal and cancer statistically different	Variable redox ratios of high-risk women combined with collagen morphology may lead to improved detection	Kirkpatrick et al.[11]
	Spatial frequency: Cancer tissues had increase in low ($\leq$10 μm^{-1}) and decrease in high (72–92 μm^{-1}) spatial frequencies		
	Redox ratio: Low risk > high risk > cancer		
Support vector machine (SVM) using GLCM, FFT	Classified cancer vs normal: Sensitivity = 81.5% Specificity = 81.1%	SVM of GLCM and FFT is moderately successful in classifying collagen alterations of cancerous tissues.	Watson et al.[34]
TPEF, SHG, and THG combined with FFT, TACS, and cellular signatures	**FFT:** Normal: 0.65 ± 0.12 Benign: 0.74 ± 0.11 Boderline: 0.80 ± 0.10 Serous: 0.79 ± 0.11	Multimodal imaging approaches are useful in classifying normal, benign, borderline, and serous ovarian tissues	Adur et al.[31]
	TACS: Normal and benign tumors demonstrate TACS-2 Serous demonstrate TACS-3		
	Cell signatures: *Number of nuclei:* Normal: 42 ± 10 Benign: 58 ± 7 Borderline:198 ± 12 Serous: 240 ± 34 *Epithelial width:* Normal: 7.54 ± 6.1.98 μm Benign: 11.52 ± 2.04 μm Borderline: 12.37 ± 4.28 μm Serous: 22.47 ± 6.17 μm		
Texton classification	Classified normal and high-grade serous with 97% accuracy	Highly specific and versatile approach to classify ovarian tissues	Wen et al.[35]
SHG creation and anisotropy (β)	Type / F_{SHG} / β Normal / 93% / 0.76 Cancer / 77% / 0.88	Cancer is denser and more organized and has better packed fibrils than normal tissues	Nadiarnykh et al.[29]
Intravital TPEF and SHG imaging using STICK objective	Intrinsic tumor fluorescence is red-shifted relative to normal; Collagen is thicker in neoplasia lesions than normal tissues	Intravital TPEF and SHG imaging provides a means to detect small neoplastic regions using both collagen and cellular features	Williams et al.[13]

of the TME in invasion and metastasis. SHG and MPE fluorescence microscopy techniques are enabling this work because of the optical sectioning, depth of penetration, and increased sensitivity and simultaneous imaging of the collagen architecture and live cell dynamics. Given this success in breast cancer, it is likely that analogous intravital techniques will advance our knowledge in the progression of ovarian cancer. This has been limited to date due to lack of robust models, but there is hope this scenario will improve. For example, as a first step, Zipfel and colleagues utilized a microendoscope STICK lens to image tumor exonografts resulting from intraperitoneal injection of OSN3 cells.[13]

Outlook for Clinical Applications/Instrumentation

Significant progress has been made in establishing SHG, by itself and in conjunction with TPEF, as a viable microscopic imaging technology to study ECM remodeling in the TME in both breast and ovarian cancer. Metrics based on collagen morphology using image processing methods, polarization analysis, and the underlying coherence of the SHG in tissues have afforded quantitative discrimination between normal and malignant tissues, using *in vitro* models and ex vivo human and animal tissues. However, much of the technology is still in the realm of the lab using large footprint microscopes and laser systems.[17] Thus, prior to clinical incorporation, the instrumentation needs

Table 3. Summary of TPEF and SHG imaging studies and techniques to probe collagen remodeling of the ECM in breast cancer.

TECHNIQUE	RESULTS			CONCLUSION	AUTHOR
FT-SHG	Type	AR		Malignant tissue has most regularly ordered fibers	Ambekar et al.[21]
	Normal	2.8 ± 1.5			
	Hyperplasia	3.5 ± 2.3			
	Dysplasia	4.5 ± 3.2			
	Malignant	11.6 ± 6.7			
Polarization-resolved SHG		Normal	Abnormal	Collagen fibers are remodeled progressively, abnormal collagen fibers only account for ~50% of malignant stroma; therefore polarization analysis has to be carefully performed to ensure discrimination	
	d_{15}/d_{31}	0.843 ± 0.064	0.064 ± 0.122		
	d_{33}/d_{31}	1.570 ± 0.074	1.603 ± 0.123		
	d_{22}/d_{31}	0.052 ± 0.043	0.117 ± 0.087		
Polarization-resolved SHG	Normal pitch angle	Diseased pitch angle		Reactive tumor stroma is not different from normal stroma.	Han et al.[53]
	51.43° ± 0.91°	50.61° ± 1.3°			
SHG creation	Type	*F/B* creation			
	Normal	34.5 ± 17			
	Abnormal	33.8 ± 7.7			
SHG creation	Type	*F/B* creation		Collagen alterations are different depending on the stage and grade of the tumor	Burke et al.[23]
	Healthy	6.0			
	IDC grade 1	5.8			
	IDC grade 2	3.5			
	IDC grade 3	3.8			
Curvelet assessment of fibers to identify TACS	Patients with TACS-3 signatures had statistically fewer months of disease-free and disease-specific survival			TACS-3 has the ability to predict patient outcome	Conklin et al.[24] Bredfeldt et al.[22,40]

improvement in terms of size and accessibility. "Turn-key" Ti:sapphire lasers and also fiber lasers with smaller footprints at specific wavelengths are now commercially available. With improvements in the power and wavelength options on the horizon, incorporation into the clinical practice, particularly for imaging of superficial tissues such as the breast, may be quickly approaching. Scanning systems have also become miniaturized. These advances have great potential for enhancing diagnostics as well as real-time determination of surgical margins, as MPE and SHG have been highly effective in delineating normal and malignant tissues.[3,10,15,22–24,29,37,53,70]

The different applications discussed here have different technology needs. For example, the FFT, curvelet transforms, and texture analysis approaches have minimal requirements for the SHG acquisition. These can be performed on highly automated slide readers that collect only the more intense forward SHG emission. This can be implemented on a cart, as a microscope stand and a large laser are not needed, where, for example, the system can comprise a simple scanning system on a stage with a small fiber laser at 780 nm. Fortuitously, commercially available fiber lasers at 785 nm are ideal for SHG excitation due to the underlying physics of SHG creation.[71]In contrast, polarization-resolved studies and also SHG directionality measurements require much more complex instrumentation and are probably limited to the lab for the near future. The simulation-based approach requires both forward and backward detection, which adds complexity and at the moment is limited to the lab setting.

SHG microendoscopy technology is also rapidly advancing, where scanning systems are becoming smaller and can achieve higher resolution.[72] This technology could be integrated into standard clinical endoscopes and laparoscopes through the instrument channel. In terms of ovarian cancer, this could be useful for the screening of women who are at higher risk of developing ovarian cancer due to *BRCA1* and/or *BRCA2* mutations. These women have a 30%–40% probability of developing ovarian cancer, compared to the 1.5% rate for the general population. As proof of principle, Williams et al used a "STICK" microendoscope to provide proof-of-concept images in their initial ovarian cancer study.[13]

Several technical limitations of microendoscope approaches remain: 1) limited field of view; however, hybrid imaging systems can be built, in which a larger field imaging modality such as optical coherence tomography or ultrasound can be used to guide the higher resolution SHG endoscopy probe; 2) limited numerical aperture (NA ~0.6); but the resolution of these devices is also increasing[73]; and 3) collection of both forward and backward SHG signals. There have been table demonstrations determining the forward SHG component in

an all backward geometry with mixed results.[63] However, with further experimentation and modeling of the SHG emission pattern, this hurdle may soon be overcome for clinical implementation. Perhaps, the largest hurdles lie in regulatory issues rather than technological challenges.

Conclusions

SHG microscopy, in conjunction with MPE fluorescence microscopy, has greatly advanced the basic understanding of the TME in breast and ovarian cancer. Recent advances in SHG instrumentation and analysis tools may allow this technique to be soon incorporated into the clinical setting for these diseases and other cancers as well. This will require collaboration with commercial instrumentation companies and also with surgeons and pathologists to adopt the new methods. Clinical use of SHG techniques may greatly enhance the state of the art in diagnosis and treatment of breast and ovarian cancer to reduce the number of cancer-related deaths. We stress that these new tools would not replace classical histology but rather would provide additional metrics to pathologists and possibly surgeons for bedside determination of tumor margins.

Author Contributions

Conceived the concepts: KT, PJC. Wrote the first draft of the manuscript: KT, PJC. Jointly developed the structure and arguments for the paper: KT, PJC. Made critical revisions and approved final version: KT, PJC. Both authors reviewed and approved of the final manuscript.

REFERENCES

1. Campagnola PJ, Clark HA, Mohler WA, Lewis A, Loew LM. Second-harmonic imaging microscopy of living cells. *J Biomed Opt*. 2001;6(3):277–86.
2. Campagnola PJ, Millard AC, Terasaki M, Hoppe PE, Malone CJ, Mohler WA. Three-dimensional high-resolution second-harmonic generation imaging of endogenous structural proteins in biological tissues. *Biophys J*. 2002;82(1 pt 1):493–508.
3. Dong CY, Campagnola PJ. Optical diagnostics of tissue pathology by multiphoton microscopy. *Expert Opin Med Diagn*. 2010;4(6):519–29.
4. Mohler W, Millard AC, Campagnola PJ. Second harmonic generation imaging of endogenous structural proteins. *Methods*. 2003;29(1):97–109.
5. Pelegati VB, Adur J, De Thomaz AA, et al. Harmonic optical microscopy and fluorescence lifetime imaging platform for multimodal imaging. *Microsc Res Tech*. 2012;75(10):1383–94.
6. Denk W, Strickler JH, Webb WW. Two-photon laser scanning fluorescence microscopy. *Science*. 1990;248:73–6.
7. Nikolenko V, Nemet B, Yuste R. A two-photon and second-harmonic microscope. *Methods*. 2003;30(1):3–15.
8. Lee KC, Siegel J, Webb SE, et al. Application of the stretched exponential function to fluorescence lifetime imaging. *Biophys J*. 2001;81(3):1265–74.
9. Provenzano PP, Rueden CT, Trier SM, et al. Nonlinear optical imaging and spectral-lifetime computational analysis of endogenous and exogenous fluorophores in breast cancer. *J Biomed Opt*. 2008;13(3):031220.
10. Skala MC, Riching KM, Bird DK, et al. In vivo multiphoton fluorescence lifetime imaging of protein-bound and free nicotinamide adenine dinucleotide in normal and precancerous epithelia. *J Biomed Opt*. 2007;12(2):024014.
11. Kirkpatrick ND, Brewer MA, Utzinger U. Endogenous optical biomarkers of ovarian cancer evaluated with multiphoton microscopy. *Cancer Epidemiol Biomarkers Prev*. 2007;16(10):2048–57.
12. Rueden CT, Conklin MW, Provenzano PP, Keely PJ, Eliceiri KW. Nonlinear optical microscopy and computational analysis of intrinsic signatures in breast cancer. *Conf Proc IEEE Eng Med Biol Soc*. 2009;2009:4077–80.
13. Williams RM, Flesken-Nikitin A, Ellenson LH, et al. Strategies for high resolution imaging of epithelial ovarian cancer by laparoscopic nonlinear microscopy. *Transl Oncol*. 2010;3(3):181–94.
14. Freund I, Deutsch M, Sprecher A. Connective tissue polarity. *Biophys J*. 1986;50:693–712.
15. Campagnola PJ, Dong CY. Second harmonic generation microscopy: principles and applications to disease diagnosis. *Lasers Photonics Rev*. 2011;5:13–26.
16. Campagnola P. Second harmonic generation imaging microscopy: applications to diseases diagnostics. *Anal Chem*. 2011;83(9):3224–31.
17. Chen X, Nadiarynkh O, Plotnikov S, Campagnola PJ. Second harmonic generation microscopy for quantitative analysis of collagen fibrillar structure. *Nat Protoc*. 2012;7(4):654–69.
18. Barsky SH, Rao CN, Grotendorst GR, Liotta LA. Increased content of Type V Collagen in desmoplasia of human breast carcinoma. *Am J Pathol*. 1982;108(3):276–83.
19. Ricciardelli C, Rodgers RJ. Extracellular matrix of ovarian tumors. *Semin Reprod Med*. 2006;24(4):270–82.
20. Adur J, Pelegati VB, de Thomaz AA, et al. Quantitative changes in human epithelial cancers and osteogenesis imperfecta disease detected using nonlinear multicontrast microscopy. *J Biomed Opt*. 2012;17(8):81401–7.
21. Ambekar R, Lau TY, Walsh M, Bhargava R, Toussaint KC Jr. Quantifying collagen structure in breast biopsies using second-harmonic generation imaging. *Biomed Opt Express*. 2012;3(9):2021–35.
22. Bredfeldt JS, Liu Y, Conklin MW, Keely PJ, Mackie TR, Eliceiri KW. Automated quantification of aligned collagen for human breast carcinoma prognosis. *J Pathol Inform*. 2014;5:28.
23. Burke K, Tang P, Brown E. Second harmonic generation reveals matrix alterations during breast tumor progression. *J Biomed Opt*. 2013;18(3):031106.
24. Conklin MW, Eickhoff JC, Riching KM, et al. Aligned collagen is a prognostic signature for survival in human breast carcinoma. *Am J Pathol*. 2011;178(3):1221–32.
25. Falzon G, Pearson S, Murison R. Analysis of collagen fibre shape changes in breast cancer. *Phys Med Biol*. 2008;53(23):6641–52.
26. Provenzano PP, Eliceiri KW, Yan L, et al. Nonlinear optical imaging of cellular processes in breast cancer. *Microsc Microanal*. 2008;14(6):532–48.
27. Zheng L, Zhuo S, Chen G, et al. Label-free discrimination of normal and fibroadenomal breast tissues using second harmonic generation imaging. *Scanning*. 2011;33(4):208–10.
28. Adur J, Pelegati VB, de Thomaz AA, et al. Optical biomarkers of serous and mucinous human ovarian tumor assessed with nonlinear optics microscopies. *PLoS One*. 2012;7(10):e47007.
29. Nadiarnykh O, LaComb RB, Brewer MA, Campagnola PJ. Alterations of the extracellular matrix in ovarian cancer studied by Second Harmonic Generation imaging microscopy. *BMC Cancer*. 2010;10:94.
30. Watson JM, Marion SL, Rice PF, et al. In vivo time-serial multi-modality optical imaging in a mouse model of ovarian tumorigenesis. *Cancer Biol Ther*. 2014;15(1):42–60.
31. Adur J, Pelegati VB, Costa LF, et al. Recognition of serous ovarian tumors in human samples by multimodal nonlinear optical microscopy. *J Biomed Opt*. 2011;16(9):096017.
32. Adur J, Pelegati VB, de Thomaz AA, et al. Second harmonic generation microscopy as a powerful diagnostic imaging modality for human ovarian cancer. *J Biophotonics*. 2014;7(1–2):37–48.
33. Haralick R, Shanmugam K, Dinstein I. Textural features for image classification. *IEEE Trans Systems Man Cybernetics*. 1973;SMC-3:610–21.
34. Watson JM, Rice PF, Marion SL, et al. Analysis of second-harmonic-generation microscopy in a mouse model of ovarian carcinoma. *J Biomed Opt*. 2012;17(7):076002.
35. Wen BL, Brewer MA, Nadiarnykh O, et al. Texture analysis applied to second harmonic generation image data for ovarian cancer classification. *J Biomed Opt*. 0001;19(9):096007. doi:10.1117/1.JBO.19.9.096007.
36. Varma M, Zisserman A. Unifying statistical texture classification frameworks. *Image Vision Comput*. 2004;22(14):1175–83.
37. Provenzano PP, Eliceiri KW, Campbell JM, Inman DR, White JG, Keely PJ. Collagen reorganization at the tumor-stromal interface facilitates local invasion. *BMC Med*. 2006;4:38.
38. Candes E, Demanet L, Donoho D, Ying LX. Fast discrete curvelet transforms. *Multiscale Model Simul*. 2006;5(3):861–99.
39. Stein AM, Vader DA, Jawerth LM, Weitz DA, Sander LM. An algorithm for extracting the network geometry of three-dimensional collagen gels. *J Microsc*. 2008;232(3):463–75.
40. Bredfeldt JS, Liu Y, Pehlke CA, et al. Computational segmentation of collagen fibers from second-harmonic generation images of breast cancer. *J Biomed Opt*. 2014;19(1):16007.
41. Deniset-Besseau A, Duboisset J, Benichou E, Hache F, Brevet PF, Schanne-Klein MC. Measurement of the second-order hyperpolarizability of the collagen triple helix and determination of its physical origin. *J Phys Chem B*. 2009;113(40):13437–45.
42. Pena AM, Boulesteix T, Dartigalongue T, Schanne-Klein MC. Chiroptical effects in the second harmonic signal of collagens I and IV. *J Am Chem Soc*. 2005;127(29):10314–22.

43. Plotnikov SV, Millard AC, Campagnola PJ, Mohler WA. Characterization of the Myosin-based source for second-harmonic generation from muscle sarcomeres. *Biophys J*. 2006;90(2):693–703.
44. Tilbury K, Lien CH, Chen SJ, Campagnola PJ. Differentiation of Col I and Col III isoforms in stromal models of ovarian cancer by analysis of second harmonic generation polarization and emission directionality. *Biophys J*. 2014;106(2):354–65.
45. Cameron GJ, Alberts IL, Laing JH, Wess TJ. Structure of type I and type III heterotypic collagen fibrils: an X-ray diffraction study. *J Struct Biol*. 2002;137(1–2):15–22.
46. Henkel W, Glanville RW. Covalent crosslinking between molecules of type I and type III collagen. The involvement of the N-terminal, nonhelical regions of the alpha 1 (I) and alpha 1 (III) chains in the formation of intermolecular crosslinks. *Eur J Biochem*. 1982;122(1):205–13.
47. Kauppila S, Bode MK, Stenback F, Risteli L, Risteli J. Cross-linked telopeptides of type I and III collagens in malignant ovarian tumours in vivo. *Br J Cancer*. 1999;81(4):654–61.
48. Liu X, Wu H, Byrne M, Krane S, Jaenisch R. Type III collagen is crucial for collagen I fibrillogenesis and for normal cardiovascular development. *Proc Natl Acad Sci USA*. 1997;94(5):1852–6.
49. Stoller P, Kim B-M, Rubinchik AM, Reiser KM, Da Silva LB. Polarization-dependent optical second-harmonic imaging of a rat-tail tendon. *J Biomed Opt*. 2001;7:205–14.
50. Chu SW, Chen SY, Chern GW, et al. Studies of (2)/(3) tensors in submicron-scaled bio-tissues by polarization harmonics optical microscopy. *Biophys J*. 2004;86:3914–22.
51. Duboisset J, Ait-Belkacem D, Roche M, Rigneault H, Brasselet S. Generic model of the molecular orientational distribution probed by polarization-resolved second-harmonic generation. *Phy Rev A*. 2012;85:4.
52. Kramer RZ, Bella J, Mayville P, Brodsky B, Berman HM. Sequence dependent conformational variations of collagen triple-helical structure. *Nat Struct Biol*. 1999;6(5):454–7.
53. Han X, Burke RM, Zettel ML, Tang P, Brown EB. Second harmonic properties of tumor collagen: determining the structural relationship between reactive stroma and healthy stroma. *Opt Express*. 2008;16(3):1846–59.
54. Prockop DJ, Fertala A. The collagen fibril: the almost crystalline structure. *J Struct Biol*. 1998;122:111–8.
55. Lacomb R, Nadiarnykh O, Townsend SS, Campagnola PJ. Phase Matching considerations in second harmonic generation from tissues: effects on emission directionality, conversion efficiency and observed morphology. *Optics Comm*. 2008;281:1823–32.
56. Nadiarnykh O, Lacomb RB, Campagnola PJ, Mohler WA. Coherent and incoherent SHG in fibrillar cellulose matrices. *Opt Express*. 2007;15(6):3348–60.
57. Ajeti V, Nadiarnykh O, Ponik SM, Keely PJ, Eliceiri KW, Campagnola PJ. Structural changes in mixed Col I/Col V collagen gels probed by SHG microscopy: implications for probing stromal alterations in human breast cancer. *Biomed Opt Express*. 2011;2(8):2307–16.
58. Birk DE. Type V collagen: heterotypic type I/V collagen interactions in the regulation of fibril assembly. *Micron*. 2001;32(3):223–37.
59. Hall G, Eliceiri KW, Campagnola PJ. Simultaneous determination of the second-harmonic generation emission directionality and reduced scattering coefficient from three-dimensional imaging of thick tissues. *J Biomed Opt*. 2013;18(11):116008.
60. Lacomb R, Nadiarnykh O, Campagnola PJ. Quantitative SHG imaging of the diseased state osteogenesis imperfecta: experiment and simulation. *Biophys J*. 2008;94:4504–14.
61. LaComb R, Nadiarnykh O, Carey S, Campagnola PJ. Quantitative SHG imaging and modeling of the optical clearing mechanism in striated muscle and tendon. *J Biomed Opt*. 2008;13:021108.
62. Mertz J, Moreaux L. Second-harmonic generation by focused excitation of inhomogeneously distributed scatterers. *Opt Commun*. 2001;196(1–6):325–30.
63. Han XX, Brown E. Measurement of the ratio of forward-propagating to back-propagating second harmonic signal using a single objective. *Opt Express*. 2010;18(10):10538–50.
64. Boas DA, Brooks DH, Miller EL, DiMarzio CA. Imaging the body with diffuse optical tomography. *IEEE Signal Proc Mag*. 2001;18(6):57–75.
65. Lehr HA, Leunig M, Menger MD, Nolte D, Messmer K. Dorsal skinfold chamber technique for intravital microscopy in nude mice. *Am J Pathol*. 1993;143(4):1055–62.
66. Condeelis J, Segall JE. Intravital imaging of cell movement in tumours. *Nat Rev Cancer*. 2003;3(12):921–30.
67. Gligorijevic B, Condeelis J. Stretching the timescale of intravital imaging in tumors. *Cell Adh Migr*. 2009;3(4):313–5.
68. Kedrin D, Gligorijevic B, Wyckoff J, et al. Intravital imaging of metastatic behavior through a mammary imaging window. *Nat Methods*. 2008;5(12):1019–21.
69. Patsialou A, Bravo-Cordero JJ, Wang Y, et al. Intravital multiphoton imaging reveals multicellular streaming as a crucial component of in vivo cell migration in human breast tumors. *Intravital*. 2013;2(2):e25294.
70. Brown E, McKee T, diTomaso E, et al. Dynamic imaging of collagen and its modulation in tumors in vivo using second-harmonic generation. *Nat Med*. 2003;9(6):796–800.
71. Hall G, Tilbury KB, Campbell KR, Eliceiri KW, Campagnola PJ. Experimental and simulation study of the wavelength dependent second harmonic generation of collagen in scattering tissues. *Opt Lett*. 2014;39(7):1897–900.
72. Wu YC, Leng YX, Xi JF, Li XD. Scanning all-fiber-optic endomicroscopy system for 3D nonlinear optical imaging of biological tissues. *Opt Express*. 2009;17(10):7907–15.
73. Zhang Y, Akins ML, Murari K, et al. A compact fiber-optic SHG scanning endomicroscope and its application to visualize cervical remodeling during pregnancy. *Proc Natl Acad Sci USA*. 2012;109(32):12878–83.